iScience

CellPress
OPEN ACCESS

Article

Microbiota regulates life-cycle transition and nematocyte dynamics in jellyfish

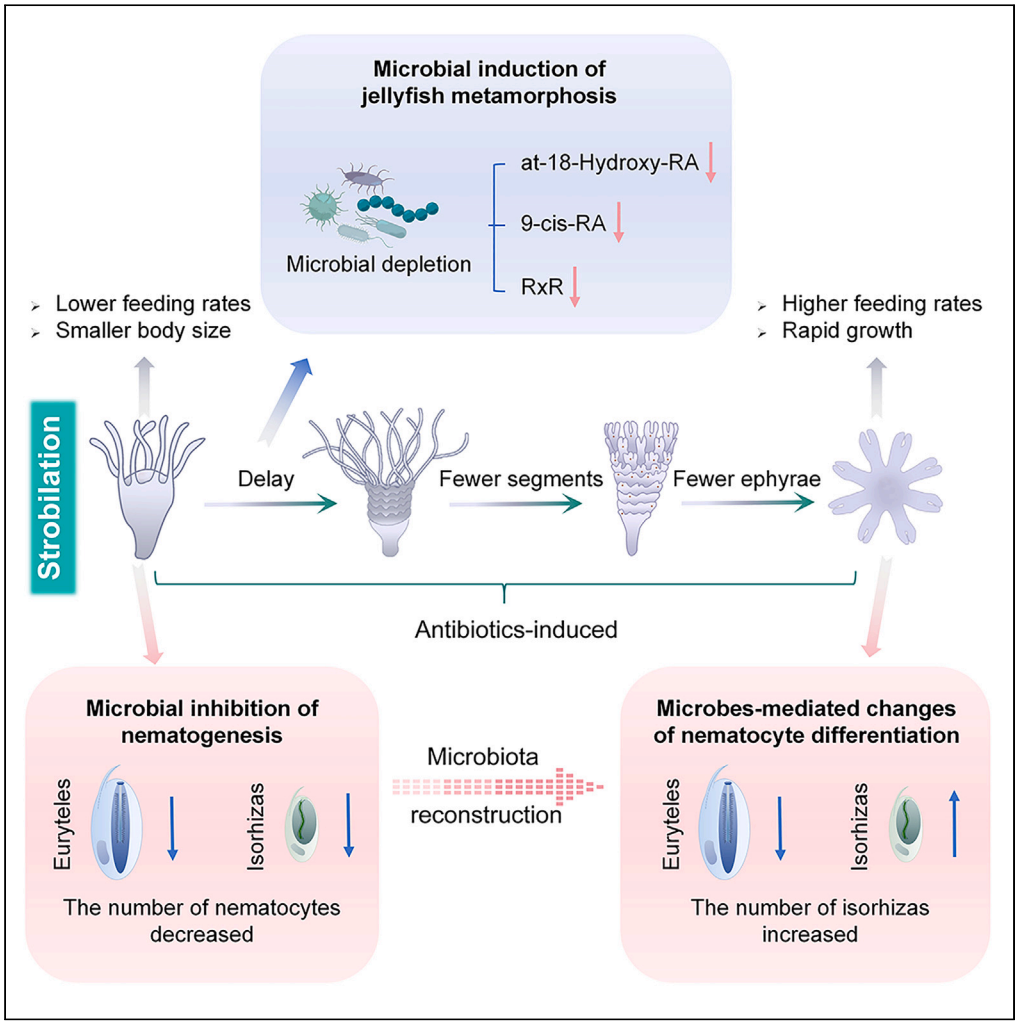

Saijun Peng, Lijing Ye, Yongxue Li, ..., Wenjin Hao, Jianmin Zhao, Zhijun Dong

zjdong@yic.ac.cn

Highlights

Microbial depletion delays the initiation of the polyp-to-medusa transition

Jellyfish-associated cyanobacteria are predicted to promote retinal synthesis

Microbial depletion results in fewer segments and ephyrae of *Aurelia*

Microbes mediate nematocyte dynamics and influence feeding and growth of jellyfish

Peng et al., iScience *26*, 108444
December 15, 2023
https://doi.org/10.1016/j.isci.2023.108444

iScience

CellPress
OPEN ACCESS

Article

Microbiota regulates life-cycle transition and nematocyte dynamics in jellyfish

Saijun Peng,[1,2,5] Lijing Ye,[1,5] Yongxue Li,[1,2] Fanghan Wang,[1,2] Tingting Sun,[1] Lei Wang,[1] Wenjin Hao,[3] Jianmin Zhao,[1,2] and Zhijun Dong[1,2,4,*]

SUMMARY

Jellyfish represent one of the most basal animal groups with complex life cycles. The polyp-to-medusa transition, termed strobilation, is the pivotal process that determines the switch in swimming behavior and jellyfish blooms. Their microbiota plays an essential role in strobilation. Here, we investigated microbiota-mediated host phenotype dynamics during strobilation in the jellyfish *Aurelia coerulea* via antibiotic-induced microbiome alteration. Microbial depletion delayed the initiation of strobilation and resulted in fewer segments and ephyrae, which could be restored via microbial recolonization. Jellyfish-associated cyanobacteria, which were eliminated by antibiotics in the polyp stage, had the potential to supply retinal and trigger the retinoic acid signaling cascade, which drove the strobilation process. The microbiota regulated nematocyte development and differentiation, influencing the feeding and growth of the jellyfish. The findings improve our understanding of jellyfish–microbe interactions and provide new insights into the role of the microbiota in shaping feeding behavior through nematocyte dynamics.

INTRODUCTION

Host-associated microbial communities play key roles in the homeostasis of metaorganisms.[1] In animals such as insects,[2–4] amphibians,[5–7] sponges,[8] and jellyfish[9–12] that undergo metamorphosis, a drastic conversion of body structures during their life, there is a corresponding restructuring of their microbial communities in response to selective pressures at specific life-cycle stages. A fascinating topic is whether and how dynamic symbionts shape specific host phenotypes at different developmental stages and influence metamorphosis. Increasing research in this field suggests that microbial consortia can affect host metamorphosis by secreting metamorphosis-inducing substances,[13,14] supplying essential amino acids and vitamins,[15–17] and suppressing opportunistic pathogen infections.[18,19] Furthermore, microbial symbionts are powerful modifiers of a series of host physiological and complex behaviors, including immunity, feeding, locomotion, mating, and cognition.[20–23]

Cnidarians, a sister group of bilaterians, are one of the most basal animal groups with life-stage transition. The life cycle of most scyphozoan jellyfish (Cnidaria) includes planula-to-polyp and polyp-to-medusa transitions (Figure 1A). The polyp-to-medusa transition, termed strobilation, is similar to metamorphosis in classic bilaterians (insects and amphibians) and relies on nuclear hormone receptors to activate the expression of metamorphosis-specific genes.[24] Previous studies have demonstrated the importance of symbiotic microbes in the strobilation, budding, and fitness of *Aurelia aurita* from the microbiota-mediated physiological changes.[12,25] The exploration of host–microbe interactions in jellyfish offers an opportunity to reveal the ancestral role of symbiotic microbes in the evolution of complex life cycles in the animal kingdom. Further, strobilation efficiently produces offspring and unlocks the jellyfish's planktonic life stage, which can lead to seasonal and catastrophic outbreaks of gelatinous jellyfish.[26] However, the microbial regulatory mechanisms underlying strobilation remain unclear.

One widely used approach for studying host–microbe interactions is manipulating the microbiome and monitoring consequent changes within the host.[27,28] Here, we selected the scyphozoan jellyfish *Aurelia coerulea*, a species renowned for its frequent global blooms, as a model organism. We used antibiotic treatment to manipulate its microbiome at the polyp stage and then recolonized the polyps with the native microbiota, examining the host phenotype. Notably, our experimental design involved some improvements over previous studies that induced strobilation by 5-methoxy-2-methyl-indole.[12,25] In nature, strobilation usually depends on temperature reduction as a trigger to initiate the process, starting in winter or early spring.[24,29] In our study, we chose cooling induction closer to natural conditions to implement the experiment to avoid the influence of the artificial addition of indole compounds on host dynamics. We investigated the microbiome-dependent phenotypes during four consecutive stages (polyp, early strobila, advanced strobila, and ephyra) using 16S rRNA gene amplicon

[1]CAS Key Laboratory of Coastal Environmental Processes and Ecological Remediation, Yantai Institute of Coastal Zone Research, Chinese Academy of Sciences, Yantai, Shandong 264003, China
[2]University of Chinese Academy of Sciences, Beijing 100049, China
[3]School of Life Science, Nantong University, Nantong, Jiangsu 226019, China
[4]Lead contact
[5]These authors contributed equally
*Correspondence: zjdong@yic.ac.cn
https://doi.org/10.1016/j.isci.2023.108444

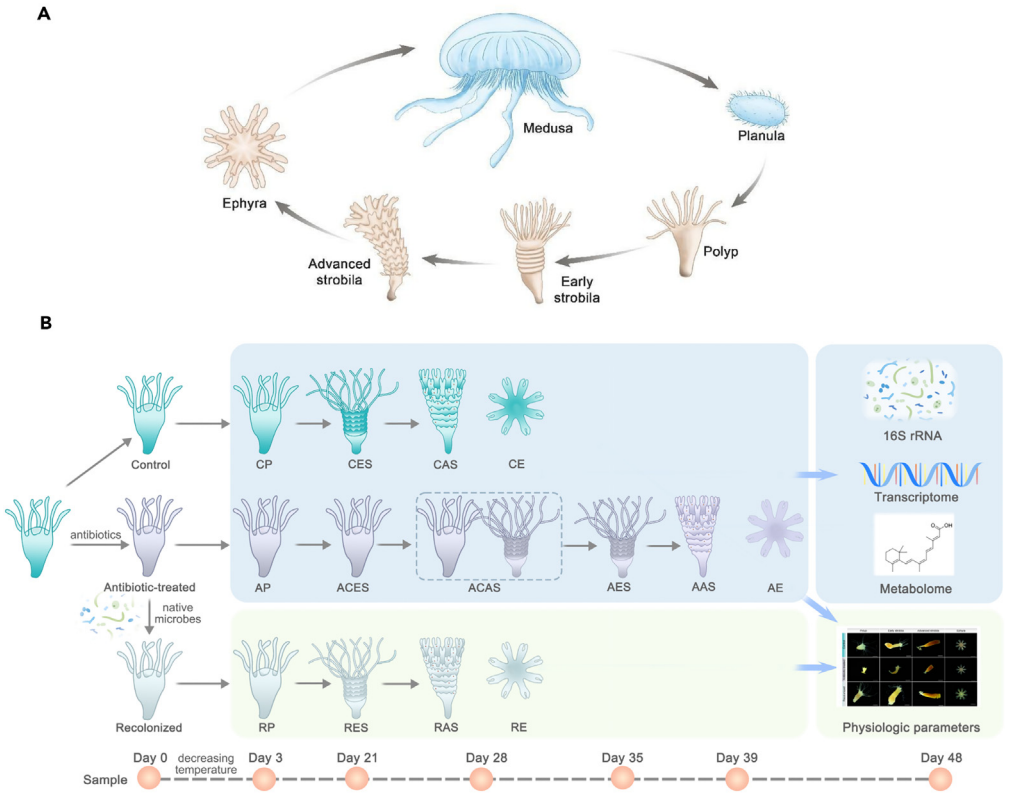

Figure 1. *Aurelia coerulea* life cycle and study design

(A) Sketch map of the life cycle of the jellyfish *A. coerulea*, in which the four stages of the strobilation process are represented in flesh color.

(B) Flow diagram of the experimental design. CP, control polyps; AP, antibiotic-treated polyps; RP, recolonized polyps. CES, control early strobilae; AES, antibiotic-treated early strobilae; RES, recolonized early strobilae; CAS, control advanced strobilae; AAS, antibiotic-treated advanced strobilae; RAS, recolonized advanced strobilae; CE, control ephyrae; AE, antibiotic-treated ephyrae; RE, recolonized ephyrae; ACES, antibiotic-treated samples collected when the control and recolonized groups reached the early strobila stage; ACAS, antibiotic-treated samples collected when the control and recolonized groups reached the advanced strobila stage.

sequencing and transcriptomic and metabolomic analyses (Figure 1B). Our findings elucidate microbial-derived retinal as a potential driver in *Aurelia* strobilation and imply the role of the microbiota in nematocyte development and differentiation.

RESULTS

Antibiotics alter the microbial community structure and composition

Settled polyps were immersed daily in an antibiotic mixture and then returned to sterile artificial seawater after 7 days. The effects of antibiotic treatment on the microbial diversity were assessed using 16S rRNA gene sequencing. The antibiotic-treated groups had lower Chao1 indexes than their corresponding control groups, with significant differences observed for the polyp and advanced strobila stages, suggesting a decrease in community richness (Student's t test, Figure 2A). Unweighted UniFrac-based principal coordinate analysis (PCoA) revealed significant changes in the microbial community structure caused by antibiotic treatment (Adonis test, Figures 2B and 2C). Dominant representatives (relative abundance >1%) in each treatment were characterized, and the compositional shifts of the dominant microbiota were visualized (Figures 2D and 2E). The relative abundances of the dominant phyla Bacteroidota and Crenarchaeota were considerably decreased in the polyp stage after antibiotic treatment (5.98%–0.19% and 1.15%–0%, respectively; Figure 2D). Compared with those in the control groups, the early and advanced strobilae in the antibiotic-treated groups had notably fewer sequences from Tenericutes but more sequences from Proteobacteria and Campylobacterota (Figure 2D). The relative abundance of Tenericutes in antibiotic-treated ephyrae (AE) was as high as 92.77%, indicating an unbalanced community composition (Figure 2D). Non-dominant phyla with relative abundances <1% were depleted in all stages after antibiotic treatment (Figure 2D). At the genus level, the dominant community composition simultaneously showed a reduction in the abundance of *Portibacter*, norank *HOC36*, norank *Kangiellaceae*, unclassified *Rhodocyclaceae*, *Sedimenticola*, *Candidatus Nitrosopumilus*, unclassified *Rhodobacteraceae*, *HTCC5015*, and unclassified *Alteromonadaceae* and an increase in the abundance of *Cobetia* and *Dokdonia* after antibiotic treatment (Figure 2E). The differential biomarkers of the control and antibiotic-treated groups at the same life stage or sampling time were screened out using linear discriminant analysis effect size (LEfSe) analysis (LDA >4, Figure 2F). These

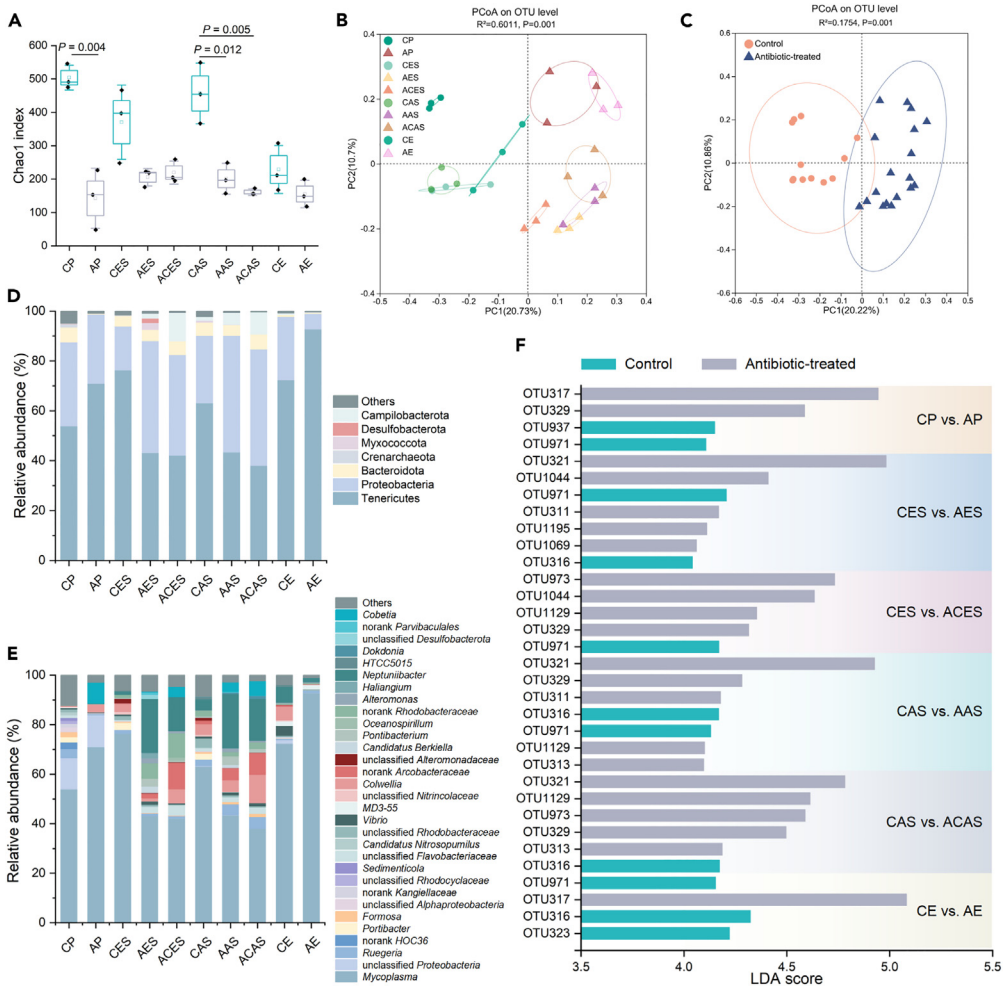

Figure 2. Antibiotic treatment significantly changes the microbial diversity and composition of *Aurelia coerulea*

(A) The Chao1 index value decreases after antibiotic treatment (Student's t test). Mean ± SD.

(B) PCoA based on unweighted-UniFrac distance reveals significant differences in the β diversity among the ten groups (Adonis tests).

(C) PCoA based on unweighted-UniFrac distance identifies significant differences in the microbial community structure between the control and antibiotic-treated groups (Adonis tests).

(D and E) Relative abundances of dominant colonizers at the phylum (D) and genus (E) levels. Only taxa with a relative abundance higher than 1% are displayed, and the rest are classified as "others".

(F) LEfSe analysis screens out biomarkers between groups collected at the same life stage or sampling time; LDA >4. The color of the bars indicates a significantly higher abundance of operational taxonomic units in the corresponding group.

differential operational taxonomic units (OTUs) are potential microbial contributors to the jellyfish phenotypic differences between the control and antibiotic-treated groups. Together, these results confirmed that antibiotic treatment affected the microbial community composition and diversity associated with *Aurelia*.

The microbial community was significantly reorganized during the progression of strobilation (Figure S1). For the control groups, the dominant colonizers on the polyps were unclassified *Proteobacteria*, *Sedimenticola*, and *Candidatus Nitrosopumilus*. The strobilae had abundant *Colwellia*, unclassified *Alteromonadaceae*, norank *Rhodobacteraceae*, and *Neptuniibacter*; the dominant microbes in the ephyrae were *Vibrio*, *MD3-55*, *Colwellia*, and *Neptuniibacter* (Figure 2E). Furthermore, the occurrence of antibiotic-treated early and advanced strobilae (AES and AAS, respectively) was accompanied by a decreased abundance of *Mycoplasma*, unclassified *Proteobacteria*, and *Cobetia* and an increased abundance of unclassified *Flavobacteriaceae*, *Vibrio*, *Candidatus Berkiella*, *Pontibacterium*, norank *Rhodobacteraceae*, *Alteromonas*, and *Neptuniibacter*. *Mycoplasma* and *MD3-55* occupied 94.63% of the planktonic AE community (Figure 2E).

Conversely, community richness was restored in recolonized *Aurelia* polyps (Student's t test, Figures S2A and S2B) and showed a community structure and composition similar to that of the control group (Adonis test, Figures S2C–S2E). The construction of the recolonization

treatment led us to conclude that the changes in physiological indicators during strobilation were due to differences in the microbial community, rather than the effects caused by antibiotics.

Microbes regulate polyp-to-medusa transition through the retinoic acid signaling pathway

Antibiotic-treated polyps displayed a 9-day delay in strobilation and decreased relative abundance of strobilae; recolonization with native microbes rescued this defect (Figures 3A and 3B), indicating the crucial role of certain microbes within the community in initiating strobilation. Moreover, the strobilae had significantly fewer segments, and fewer ephyrae were released in the antibiotic-treated group (one-way analysis of variance [ANOVA]; Figures 3C and 3D).

The mechanism underlying metamorphosis induction was explored by comparing the control polyps (CP) with antibiotic-treated polyps (AP) and control early strobilae (CES) with antibiotic-treated samples collected when the control and recolonized groups reached the early strobila stage (ACES). The top three Kyoto Encyclopedia of Genes and Genomes (KEGG) pathways co-enriched with differentially expressed genes (DEGs) and differentially expressed metabolites (DEMs) suggested a potential role of the retinol metabolism pathway (ko00830; Figure 3E, Table S1). Members of the retinoic acid (RA) signaling cascade are known to be involved in the initiation of *Aurelia* strobilation in response to temperature changes.[24] Transcriptomic analysis revealed non-significant differences or upregulation trends in *BCO1*, *RDH2*, and *CYP26A* expression in the antibiotic-treated group (Figures 3F–3H). However, the expression of the RxRα-encoding gene was downregulated in ACES compared with that in CES (Figure 3I). Moreover, the relative abundances of 9-cis-RA and all-trans-18-hydroxy-RA, involved in RA signaling, decreased significantly in AP and ACES (Figures 3J and 3K, Table S1). A decrease in 9-cis-RA levels can inhibit the activation of the RxRα receptor, leading to a delay in strobilation.[24] These findings suggest that microbes regulate the retinal synthesis pathway and hence affect the production of downstream signaling metabolites, instead of directly acting on the RA cascade.

PICRUSt2 analysis of 16S rRNA gene sequences revealed the functional potential of *Aurelia*-associated unclassified *Cyanobacteria* (OTU259) in encoding all-trans-8′-apo-β-carotenal 15,15′-oxygenase (Diox1) and CruA/CruP-type lycopene cyclases (Table S2). Furthermore, the genes encoding these enzymes were absent from the *A. coerulea* genome (NCBI BioProject: PRJNA1005405). Unclassified *Cyanobacteria* (OTU259) was a non-dominant colonizer with a relative abundance of <1%, and its mean relative abundance in the polyp stage decreased from 0.685% in CP to 0.002% in AP (Figure 3L). The predicted KO abundances of *Diox1*, *CruA*, and *CruP* were significantly downregulated in AP (Student's t test, Figure 3M). Combined with KEGG pathway analysis, we predicted two potential pathways for unclassified *Cyanobacteria* to promote the expression of RA signaling metabolites before the beginning of strobilation (Figure 3N). In detail, unclassified *Cyanobacteria* could synthesize beta carotene through the action of CruA and CruP. In the antibiotic-treated group, carotene synthesis was greatly reduced in the polyp stage, in turn leading to a decrease in the abundance of downstream 9-cis-RA and all-trans-18-hydroxy-RA (Figure 3N). Alternatively, unclassified *Cyanobacteria* could convert β-apo-carotenal into retinal by producing Diox1; thus, the loss of unclassified *Cyanobacteria* would cause retinal deprivation and similarly induce inhibition of RA synthesis (Figure 3N).

Gene Ontology (GO) analysis of all *A. coerulea* genes identified 20 GO terms related to somites and segments in bilaterians, suggesting a molecular similarity in segmentation between basal *Aurelia* and bilaterians (Figures S3A and S3B). Gene set enrichment analysis (GSEA) of the aforementioned GO terms between CES and AES enriched five terms—segmentation, somite development, segment specification, blastoderm segmentation, and segment polarity determination—which were generally upregulated in AES (NES >1); the enrichment of segmentation (GO: 0035282) was the most significant ($p < 0.05$, $q < 0.25$; Figures S3C and S3D). This suggests that changes in the expression of conserved genes related to segments and somites are not the main reason for the lower number of segments observed in the AES. Reportedly, segmentation in *Aurelia* is correlated with polyp size.[30]

Microbes are correlated with nematocyte dynamics during polyp-to-medusa transition

The sizes of polyps and newly released ephyrae (day 1) were significantly smaller in the antibiotic-treated group than in the control group (one-way ANOVA, Figures 4A and 4B); however, AE displayed a rapid growth phenotype after release, and their sizes exceeded those of control ephyrae (CE) on day 3 (Figure 4B). Concurrently, the feeding rate of AP was significantly lower than that of CP, whereas that of AE was higher than that of CE and reached statistical significance on day 3 (one-way ANOVA, Figures 4C and 4D). The size and feeding rate of the recolonized group were similar to those of the control group, confirming a dominant influence of the microbes (one-way ANOVA, Figures 4A–4D). Therefore, the feeding rate was the major factor leading to size differences.

Next, we determined morphological and quantitative changes in nematocytes (Figures 4E–4I), which play a key role in the feeding behavior of *Aurelia*. Nematocytes of *Aurelia* are divided into two types, according to the morphology of nematocysts, namely euryteles and isorhizas,[31] but no significant morphological differences were observed among the treatment groups (Figure 4E). Microscopic analysis of the nematocytes at the base of the tentacles and marginal lappets of the polyps and ephyrae, respectively (Figures 4F and 4G), indicated that the number of euryteles and isorhizas was significantly lower in AP than in CP or recolonized polyps (RP; one-way ANOVA, Figure 4H). On day 3 after release, euryteles maintained a low-density distribution in AE, but the number of isorhizas increased significantly and was higher in AE than in CE or recolonized ephyrae (RE; one-way ANOVA, Figure 4I). Therefore, we speculate that the early development and differentiation of nematocytes were affected by microbes.

We analyzed changes in nematocytes at the transcriptional level, and the results revealed 18 DEGs (Figure 4J). To verify the nematocyte specificity of these DEGs, we performed single-cell RNA sequencing of CE and identified cluster 1 as nematocytes based on gene expression patterns (Figures S4A and S4B, Table S3, Data S1). The UMAP plots of the 18 genes selected in this study were used to visualize the cell clusters in which they were expressed, and they were finally determined to be nematocyte-specific (Figure S4C).

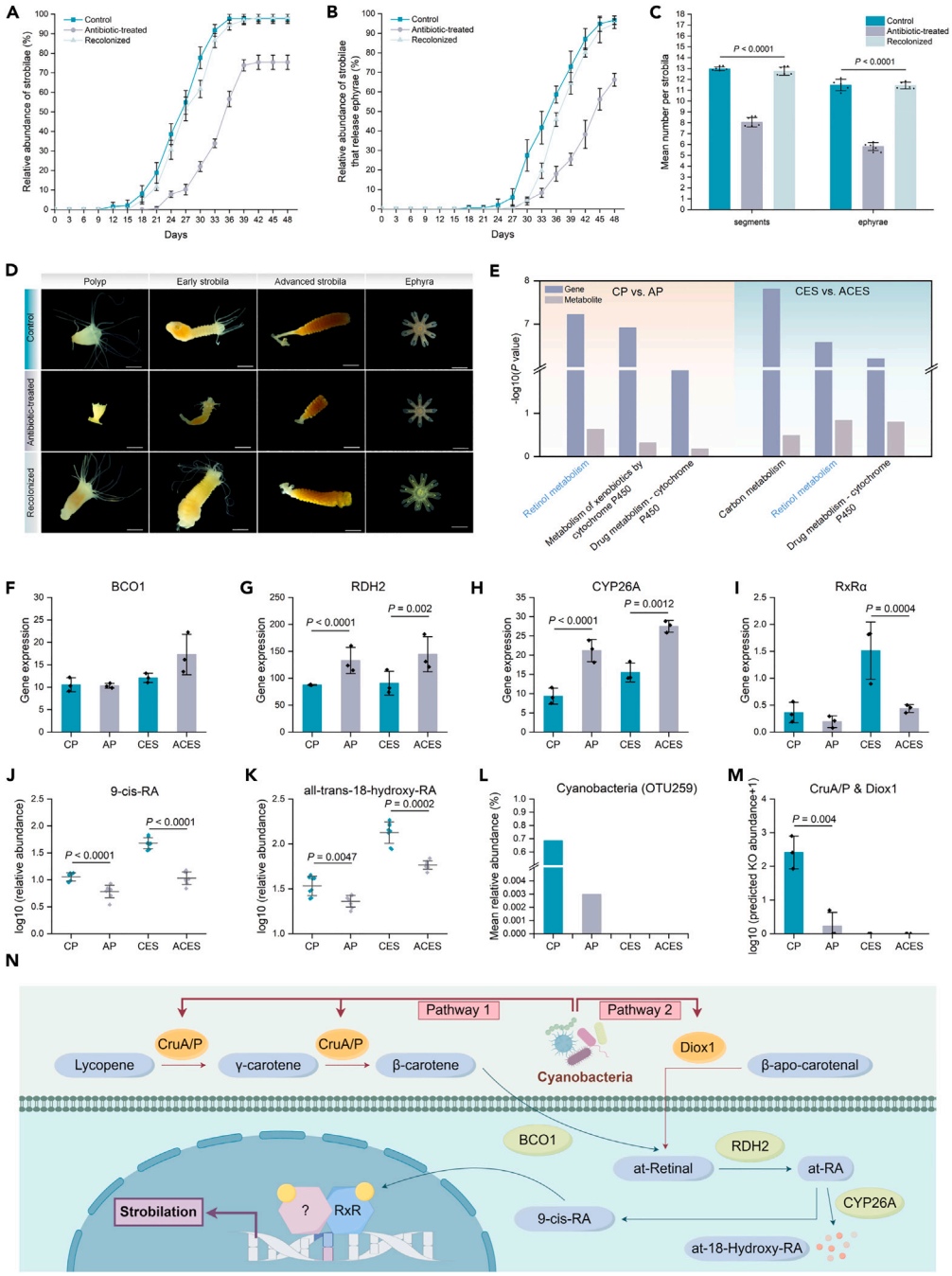

Figure 3. Microbial reduction leads to delayed strobilation and fewer segments in *Aurelia coerulea*

(A and B) Relative abundances of total strobilae (A) and advanced strobilae (B), monitored every 3 days.

(C) Number of segments per animal and ephyrae released per animal during the 48-day experiment (one-way ANOVA and Fisher's LSD test).

(D) Photographs of the morphological stages of *A. coerulea*. Scale bar, 1 mm.

(E) Top three KEGG pathways with the largest number of differentially expressed genes and metabolites (DEGs and DEMs, respectively).

(F–I) FPKM expression of DEGs. The p-value refers to the corrected FDR value.

(J and K) Relative abundances of two DEMs involved in retinoic acid (RA) signaling (Student's t test). See also Table S1.

(L) Mean relative abundance (%) of unclassified *Cyanobacteria* (OTU259).

(M) Predicted KO abundances of *Diox1* and *CruA/P* based on PICRUSt2 transformed into the log10 (x + 1) (Student's t test). See also Table S2.

(N) Two potential pathways for associated cyanobacteria regulating RA signaling. The predicted pathway diagram was generated via Figdraw (https://www.figdraw.com). CruA/P, lycopene cyclases CruA and CruP; Diox1, all-trans-8′-apo-β-carotenal 15,15′-oxygenase; BCO1, beta carotene 15,15′-dioxygenase; RDH2, retinol dehydrogenase 2; CYP26A, cytochrome P450 family 26 subfamily A; at-retinal, all-trans-retinal; at-RA, all-trans-retinoic acid; 9-cis-RA, 9-cis-retinoic acid; at-18-Hydroxy-RA, all-trans-18-hydroxyretinoic acid. All data are represented as mean ± SD.

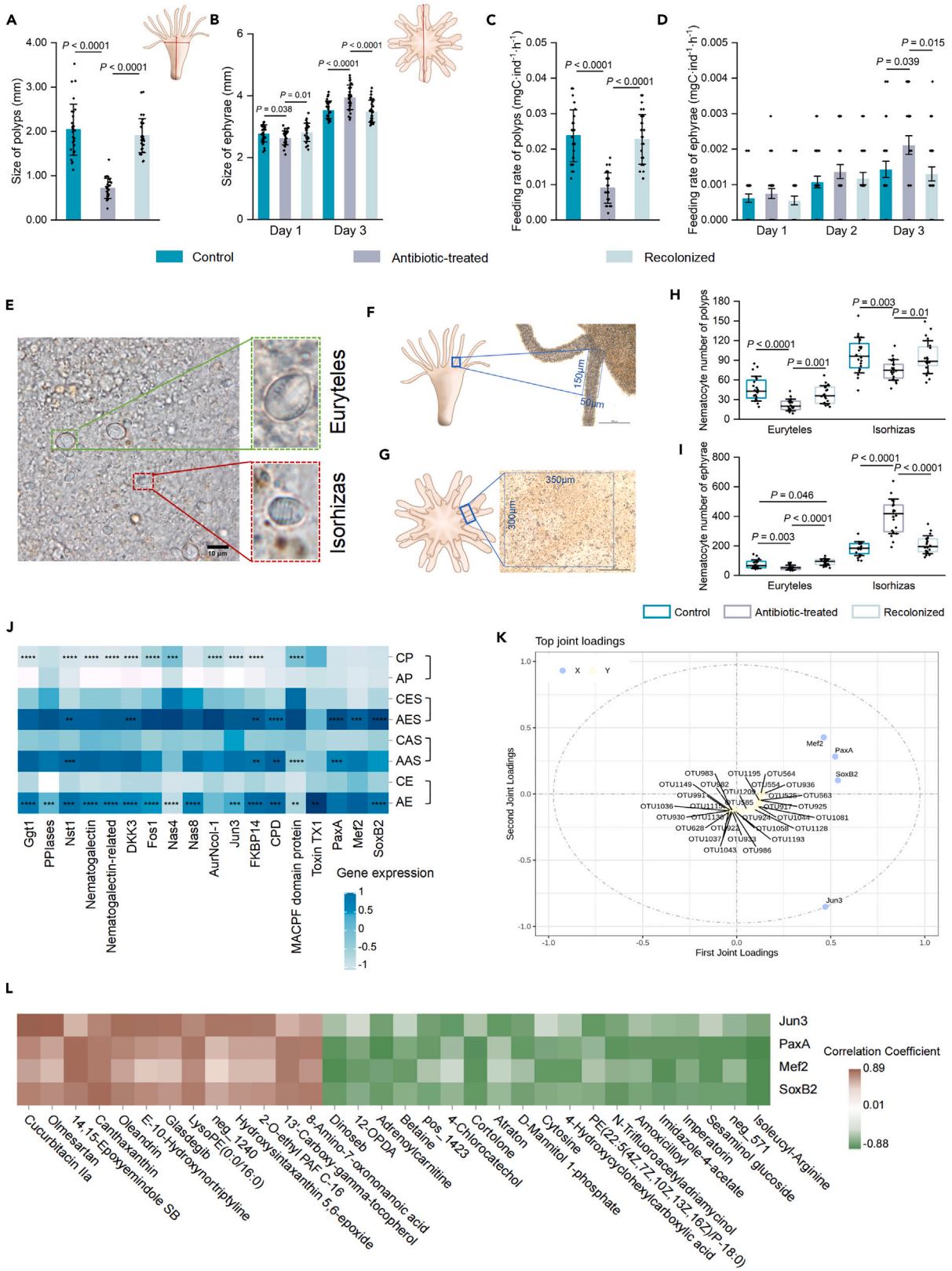
A
B
C
D
Size of polyps (mm)
Size of ephyrae (mm)
Feeding rate of polyps (mgC·ind⁻¹·h⁻¹)
Feeding rate of ephyrae (mgC·ind⁻¹·h⁻¹)
P < 0.0001
P = 0.01
P = 0.038
P = 0.039
P = 0.015
Day 1
Day 2
Day 3
Control
Antibiotic-treated
Recolonized
E
Euryteles
Isorhizas
10 μm
F
150μm
50μm
G
350μm
300μm
H
Nematocyte number of polyps
P = 0.003
P = 0.01
P = 0.001
I
Nematocyte number of ephyrae
P = 0.046
J
CP
AP
CES
AES
CAS
AAS
CE
AE
Ggt1
PPIases
Nst1
Nematogalectin
Nematogalectin-related
DKK3
Fos1
Nas4
Nas8
AurNcol-1
Jun3
FKBP14
CPD
MACPF domain protein
Toxin TX1
PaxA
Mef2
SoxB2
Gene expression
K
Top joint loadings
Second Joint Loadings
First Joint Loadings
Mef2
PaxA
SoxB2
Jun3
L
Jun3
PaxA
Mef2
SoxB2
Correlation Coefficient
Cucurbitacin IIa
Olmesartan
14,15-Epoxyemindole SB
Canthaxanthin
Oleandrin
E-10-Hydroxynortriptyline
Glasdegib
LysoPE(0:0/16:0)
neg_1240
Hydroxysintaxanthin 5,6-epoxide
2-O-ethyl PAF C-16
13'-Carboxy-gamma-tocopherol
8-Amino-7-oxononanoic acid
Dinoseb
12-OPDA
Adrenoylcarnitine
Betaine
pos_1423
4-Chlorocatechol
Cortolone
Atraton
D-Mannitol 1-phosphate
Cytosine
4-Hydroxycyclohexylcarboxylic acid
PE(22:5(4Z,7Z,10Z,13Z,16Z)/P-18:0)
N-Trifluoroacetyladriamycinol
Amoxicillinyl
Imidazole-4-acetate
Imperatorin
Sesaminol glucoside
neg_571
Isoleucyl-Arginine

Figure 4. Microbial colonizers affect feeding and body size by mediating changes in nematocytes of *Aurelia coerulea*

(A and B) Body sizes of polyps (A) and ephyrae (B) (one-way ANOVA and Fisher's LSD test); mean ± SD. The red line in the upper right corner indicates the area where the body sizes were measured. The size of each polyp was determined by multiplying length by width.

(C and D) Feeding rates of polyps (C) and ephyrae (D) and those in ephyra stage were measured on the days 1, 2, and 3 after release, respectively (one-way ANOVA and Fisher's LSD test). Data in (C) are represented as mean ± SD and data in (D) as mean ± SE.

(E) Morphological imaging of nematocytes. Scale bar, 10 μm.

(F) Number of nematocytes in each polyp within the indicated rectangular area (150 × 50 μm) at an extended tentacle base. The right side is the actual view. Scale bar, 100 μm.

(G) Number of nematocytes in each ephyra within the indicated rectangular area (300 × 350 μm) at a flat marginal lappet base. The right side is the actual view. Scale bar, 100 μm.

(H and I) Number of nematocytes in polyps (H) and ephyrae on day 3 after release (I) (one-way ANOVA and Fisher's LSD test); mean ± SD.

(J) FPKM expression of 18 nematocyte-specific genes. p-value refers to the corrected FDR value. The asterisk indicates significantly higher gene expression after pairwise comparison; **$p < 0.01$; ***$p < 0.001$; ****$p < 0.0001$. See also Figure S4.

(K) The O2PLS model analyzes the variable correlation of the expression of four nematogenesis-related genes and the differential operational taxonomic units.

(L) Spearman correlation analysis reveals differential metabolites that are strongly correlated with four nematogenesis-related genes (correlation coefficient >0.8 and $p < 0.05$). See also Table S1.

The expression of *Jun3*, involved in normal nematogenesis,[32] was significantly decreased in AP and elevated from AES to AE. The expression of other genes linked to nematogenesis, *PaxA*, *Mef2*, and *SoxB2*,[33] was also upregulated from AES to AE (Figure 4J). The expression of *Ggt1*, *Nematogalectin*, and *AurNcol-1*, which maintain nematocyst structure and discharge,[33–35] was considerably downregulated in AP but upregulated to different degrees from AES to AE, compared with that in the same stages of the control group (Figure 4J). Similarly, the expression of *DKK3*, *Nas4*, *Nas8*, *MACPF domain protein*, and *Toxin TX1*, encoding nematocyst venom proteins,[34,36] was downregulated in AP and elevated thereafter, compared with that in the same stage of the control treatment (Figure 4J). These results support the hypothesis that microbes mediate molecular changes in *Aurelia* nematocytes.

The O2PLS model was used to analyze the variable correlation of the expression of four DEGs (*Jun3*, *PaxA*, *Mef2*, and *SoxB2*) related to nematogenesis and differential OTUs. The top five differential and dominant OTUs linked with changes in nematocytes were unclassified *Flavobacteriaceae* (OTU1128), *Phaeobacter porticola* (OTU1044), unclassified *Rhodobacteraceae* (OTU933), *Alteromonas* (OTU925), and *Candidatus Berkiella* (OTU1195; Figure 4K). Moreover, spearman correlation analysis was performed between four DEGs (*Jun3*, *PaxA*, *Mef2*, and *SoxB2*) and DEMs, and remarkably correlative DEMs were deciphered (correlation coefficients >0.8, $p < 0.05$; Figure 4L, Table S1).

DISCUSSION

Jellyfish are informative model species in basal metazoans, receiving extensive attention for their evolutionary position and ecological significance.[37] The life cycle of Medusozoa from sessile polyp to motile medusa stages, termed strobilation, is a pivotal process that determines swimming behavior and jellyfish blooms.[29] Although a microbial influence on the transition processes has been proposed, the mechanisms involved remain poorly understood.[12,25]

Herein, we report that antibiotic-induced microbiome depletion delays the initiation of strobilation, which is consistent with the findings of Weiland-Bräuer et al.[12] The RA signaling pathway enables to drive the transition from polyps to jellyfish in *Aurelia*.[24] In our study, a decrease in *RxR* expression and 9-cis-RA abundance was detected in the antibiotic-treated samples prior to the onset of strobilation, which may be a major reason for its delay after antibiotic treatment. Similarly, downregulated expression of *RxR* was observed in sterile *A. aurita*.[25] We conclude that associated microbes play a key role in the initiation of strobilation in *Aurelia*. However, the molecular patterns of microbes associated with *Aurelia* that participate in the modulation of RA signaling remain unknown. Subsequently, we predicted two potential pathways by which associated unclassified *Cyanobacteria* produce retinal and hence affect downstream RA signaling, based on PICRUSt2 analysis. Although the targeted cyanobacteria were not the dominant taxa in our study, there are scenarios in which low-abundance members of the microbial community play an important role.[38] Cyanobacteria are widely associated with sponges,[39–41] corals,[42] ascidians,[43,44] and jellyfish,[45–48] but these interactions are not completely understood. In non-symbiosis, partial free-living cyanobacteria synthesize RA and carotene by encoding enzymes or via non-enzymatic methods (e.g., free radical oxidation) and thus exert potential teratogenic effects on aquatic residents.[49–52] Cyanobacterial retinal-forming via Diox1 and CruA/CruP enzymes has been functionally identified in several species.[53,54] In the case of symbiosis, *Prochloron* sp., a cyanobacterium, protects its ascidian host from active forms of oxygen by producing superoxide dismutase.[55] It seems logical that cyanobacteria, as associated bacteria, can promote the RA pathway of jellyfish by presumably enzymatic methods. This prediction enlightens us to consider the potential ecological relationship between the regional concentration of cyanobacteria and strobilation or even outbreaks of jellyfish.

Our analyses demonstrate that microbial dynamics profoundly alter nematocyte development during the polyp-to-medusa transition in *Aurelia*. Nematocyte, a defining feature of cnidarians, is a highly specialized evolutionary novelty that enables prey capture and defense.[35] An optimized method distinguished two major types of nematocysts in *Aurelia*, euryteles and isorhizas.[31] Euryteles with large capsule volume and toxin storage are "armor-breaking" weapons, specialized for prey capturing, whereas isorhizas are an ancestral type, with smaller sizes and unspined tubules, which are supposed to entangle prey.[31,56] Herein, nematocyte distribution was sparse in AP compared with that in CP, which affected the ability of the polyps to capture *Artemia* nauplii. The initiation of strobilation caused a restructuring of the microbial community that contributed to an excessive development of isorhizas in the antibiotic-treated group, improving the predation ability of AE. These findings improve our understanding of the microbial regulation of nematocyte development and differentiation in cnidarians. A pioneering

study showed that nematocytes of the sea anemone *Nematostella vectensis* evolved from a specific subtype of neurons under the drive of the regulatory gene ZNF845.[57] In bilaterians, the interaction among gut microbes, the nervous system, and animal behavior is extensively known.[20,27,58,59] Recently, it was reported that the microbiota actively regulates the nervous system and affects host behavior in cnidarians, especially in *Hydra*.[38] Some studies on the interaction between neurons and microbes may hint toward a link between nematocytes and microbes because nematocytes are Cnidaria-specific mechanosensory cells. From the perspective of the ecosystem, the disturbance of jellyfish feeding behavior modulated by nematocytes could directly affect the survival of zooplankton prey, including fish eggs and larvae, and competitively impact the population of animals at the same trophic level, such as fish.[60] In addition, jellyfish feeding diverts zooplankton production away from the upper trophic level, with one study showing that only 2% of the energy consumed by jellyfish was transferred to the upper trophic level, most of which was lost to detritus.[61] Therefore, changes in jellyfish predation could trigger trophic cascades in pelagic food webs and disturb the energy flow of the ecosystem.

A decrease was observed in the number of segments and ephyrae in antibiotic-treated *A. coerulea*, consistent with previous studies on *A. aurita*.[12,25] Kroiher et al.[30] identified a positive correlation between polyp size and the number of segments of *Aurelia*. Thus, the reduced number of segments in our study was assumed to be due to the reduced polyp size after antibiotic treatment, which may be due to feeding inhibition caused by microbial-induced nematocyte developmental disorders. As a typical representative of polydisc strobilation, wherein multiple ephyrae are produced from one strobila, the number of released ephyrae in *Aurelia* may largely determine the initial population size of medusae, which is linked to bloom potential.[26,62] Therefore, this knowledge is of ecological importance and may be propitious to the microbial control of jellyfish blooms in the future.

Limitations of the study

Considering the short reads of 16S rRNA gene amplicon sequencing and the possible accuracy error of PICRUSt2 functional prediction, we acknowledge that more in-depth experiments, such as fluorescence *in situ* hybridization for cyanobacteria-related tissue localization and genome assembly of targeted cyanobacteria, are necessary to confirm the prediction for associated cyanobacteria in the future. Moreover, microbial taxa responsible for nematocyte dynamics are still ambiguous. The isolation and purification of native strains from jellyfish are expected to identify specific microbes that can rescue nematocyte abnormalities. Finally, we established the recolonized polyp model to determine the phenotypic responses to microbiome alternation. However, due to the technical limitations of the current sterile polyp model construction, antibiotics have been introduced into the experiment and may have potential effects on the host.

STAR★METHODS

Detailed methods are provided in the online version of this paper and include the following:

- KEY RESOURCES TABLE
- RESOURCE AVAILABILITY
  - Lead contact
  - Materials availability
  - Data and code availability
- EXPERIMENTAL MODEL AND STUDY PARTICIPANT DETAILS
  - Animal use ethics
  - Husbandry of *Aurelia coerulea*
  - Generation of sterile *Artemia* nauplii
  - Generation of control, antibiotic-treated and recolonized polyps
- METHOD DETAILS
  - Physiological parameters
  - Sample collection of multi-omics sequencing
  - 16S rRNA gene amplicon sequencing and data analysis
  - Transcriptome sequencing and analysis
  - LC-MS analysis
  - Single-cell RNA sequencing
  - Nematocyte imaging and quantification
- QUANTIFICATION AND STATISTICAL ANALYSIS

SUPPLEMENTAL INFORMATION

Supplemental information can be found online at https://doi.org/10.1016/j.isci.2023.108444.

ACKNOWLEDGMENTS

This work was supported by grants from the Key Project of NSFC-Shandong Joint Fund (U2106208), the National Science & Technology Fundamental Resources Investigation Program of China (2022FY100600), the National Natural Science Foundation of China (41876138),

the Strategic Priority Research Program of the Chinese Academy of Sciences (XDA23050301), and the Taishan Scholars Program (tsqn202211263).

AUTHOR CONTRIBUTIONS

S.J.P., L.J.Y., Y.X.L., F.H.W., T.T.S., and L.W. performed the experiments. S.J.P., L.J.Y., Y.X.L., F.H.W., W.J.H., and J.M.Z. performed the bioinformatics analysis. S.J.P. and Z.J.D. wrote the manuscript. Z.J.D. conceived and designed the study. All authors reviewed and contributed to the final manuscript.

DECLARATION OF INTERESTS

The authors declare no competing interests.

INCLUSION AND DIVERSITY

We support inclusive, diverse, and equitable conduct of research.

Received: October 3, 2023
Revised: October 25, 2023
Accepted: November 9, 2023
Published: November 19, 2023

REFERENCES

1. Morais, L.H., Schreiber, H.L., and Mazmanian, S.K. (2021). The gut microbiota-brain axis in behaviour and brain disorders. Nat. Rev. Microbiol. *19*, 241–255.
2. Yun, J.-H., Roh, S.W., Whon, T.W., Jung, M.-J., Kim, M.-S., Park, D.-S., Yoon, C., Nam, Y.-D., Kim, Y.-J., Choi, J.-H., et al. (2014). Insect Gut Bacterial Diversity Determined by Environmental Habitat, Diet, Developmental Stage, and Phylogeny of Host. Appl. Environ. Microbiol. *80*, 5254–5264.
3. Shukla, S.P., Sanders, J.G., Byrne, M.J., and Pierce, N.E. (2016). Gut microbiota of dung beetles correspond to dietary specializations of adults and larvae. Mol. Ecol. *25*, 6092–6106.
4. Wang, X., Gao, Q., Wang, W., Wang, X., Lei, C., and Zhu, F. (2018). The gut bacteria across life stages in the synanthropic fly *Chrysomya megacephala*. BMC Microbiol. *18*, 131.
5. Kohl, K.D., Cary, T.L., Karasov, W.H., and Dearing, M.D. (2013). Restructuring of the amphibian gut microbiota through metamorphosis. Environ. Microbiol. Rep. *5*, 899–903.
6. Bates, K.A., Clare, F.C., O'Hanlon, S., Bosch, J., Brookes, L., Hopkins, K., McLaughlin, E.J., Daniel, O., Garner, T.W.J., Fisher, M.C., and Harrison, X.A. (2018). Amphibian chytridiomycosis outbreak dynamics are linked with host skin bacterial community structure. Nat. Commun. *9*, 693.
7. Fontaine, S.S., Mineo, P.M., and Kohl, K.D. (2021). Changes in the gut microbial community of the eastern newt (*Notophthalmus viridescens*) across its three distinct life stages. FEMS Microbiol. Ecol. *97*, fiab021.
8. Fieth, R.A., Gauthier, M.-E.A., Bayes, J., Green, K.M., and Degnan, S.M. (2016). Ontogenetic Changes in the Bacteria Symbiont Community of the Tropical Demosponge *Amphimedon queenslandica*: Metamorphosis Is a New Beginning. Front. Mar. Sci. *3*, 228.
9. Weiland-Bräuer, N., Neulinger, S.C., Pinnow, N., Künzel, S., Baines, J.F., and Schmitz, R.A. (2015). Composition of Bacterial Communities Associated with *Aurelia aurita* Changes with Compartment, Life Stage, and Population. Appl. Environ. Microbiol. *81*, 6038–6052.
10. Lee, M.D., Kling, J.D., Araya, R., and Ceh, J. (2018). Jellyfish Life Stages Shape Associated Microbial Communities, While a Core Microbiome Is Maintained Across All. Front. Microbiol. *9*, 1534.
11. Hao, W., Gerdts, G., Holst, S., and Wichels, A. (2019). Bacterial communities associated with scyphomedusae at Helgoland Roads. Mar. Biodivers. *49*, 1489–1503.
12. Weiland-Bräuer, N., Pinnow, N., Langfeldt, D., Roik, A., Güllert, S., Chibani, C.M., Reusch, T.B.H., and Schmitz, R.A. (2020). The Native Microbiome is Crucial for Offspring Generation and Fitness of *Aurelia aurita*. mBio *11*, e02336-20.
13. Paludo, C.R., Menezes, C., Silva-Junior, E.A., Vollet-Neto, A., Andrade-Dominguez, A., Pishchany, G., Khadempour, L., do Nascimento, F.S., Currie, C.R., Kolter, R., et al. (2018). Stingless Bee Larvae Require Fungal Steroid to Pupate. Sci. Rep. *8*, 1122.
14. Song, H., Hewitt, O.H., and Degnan, S.M. (2021). Arginine Biosynthesis by a Bacterial Symbiont Enables Nitric Oxide Production and Facilitates Larval Settlement in the Marine-Sponge Host. Curr. Biol. *31*, 433–437.e3.
15. Rio, R.V.M., Symula, R.E., Wang, J., Lohs, C., Wu, Y.n., Snyder, A.K., Bjornson, R.D., Oshima, K., Biehl, B.S., Perna, N.T., et al. (2012). Insight into the Transmission Biology and Species-Specific Functional Capabilities of Tsetse (Diptera: Glossinidae) Obligate Symbiont *Wigglesworthia*. mBio *3*, e00240-11.
16. Klein, A., Schrader, L., Gil, R., Manzano-Marín, A., Flórez, L., Wheeler, D., Werren, J.H., Latorre, A., Heinze, J., Kaltenpoth, M., et al. (2016). A novel intracellular mutualistic bacterium in the invasive ant *Cardiocondyla obscurior*. ISME J. *10*, 376–388.
17. Anbutsu, H., Moriyama, M., Nikoh, N., Hosokawa, T., Futahashi, R., Tanahashi, M., Meng, X.-Y., Kuriwada, T., Mori, N., Oshima, K., et al. (2017). Small genome symbiont underlies cuticle hardness in beetles. Proc. Natl. Acad. Sci. USA *114*, E8382–E8391.
18. Kaltenpoth, M., Göttler, W., Herzner, G., and Strohm, E. (2005). Symbiotic bacteria protect wasp larvae from fungal infestation. Curr. Biol. *15*, 475–479.
19. Engl, T., Kroiss, J., Kai, M., Nechitaylo, T.Y., Svatoš, A., and Kaltenpoth, M. (2018). Evolutionary stability of antibiotic protection in a defensive symbiosis. Proc. Natl. Acad. Sci. USA *115*, E2020–E2029.
20. Schretter, C.E., Vielmetter, J., Bartos, I., Marka, Z., Marka, S., Argade, S., and Mazmanian, S.K. (2018). A gut microbial factor modulates locomotor behaviour in *Drosophila*. Nature *563*, 402–406.
21. Lynch, J.B., and Hsiao, E.Y. (2019). Microbiomes as sources of emergent host phenotypes. Science *365*, 1405–1409.
22. Buffington, S.A., Dooling, S.W., Sgritta, M., Noecker, C., Murillo, O.D., Felice, D.F., Turnbaugh, P.J., and Costa-Mattioli, M. (2021). Dissecting the contribution of host genetics and the microbiome in complex behaviors. Cell *184*, 1740–1756.e16.
23. Chu, C., Murdock, M.H., Jing, D., Won, T.H., Chung, H., Kressel, A.M., Tsaava, T., Addorisio, M.E., Putzel, G.G., Zhou, L., et al. (2019). The microbiota regulate neuronal function and fear extinction learning. Nature *574*, 543–548.
24. Fuchs, B., Wang, W., Graspeuntner, S., Li, Y., Insua, S., Herbst, E.-M., Dirksen, P., Böhm, A.M., Hemmrich, G., Sommer, F., et al. (2014). Regulation of Polyp-to-Jellyfish Transition in *Aurelia aurita*. Curr. Biol. *24*, 263–273.
25. Jensen, N., Weiland-Bräuer, N., Joel, S., Chibani, C.M., and Schmitz, R.A. (2023). The Life Cycle of *Aurelia aurita* Depends on the Presence of a Microbiome in Polyps Prior to Onset of Strobilation. Microbiol. Spectr. *11*, e00262-23.
26. Wang, N., Li, C., Wang, Y., and Feng, S. (2018). Carbon distribution strategy of *Aurelia coerulea* polyps in the strobilation process in relation to temperature and food supply. J. Oceanol. Limnol. *36*, 2216–2230.

27. Serger, E., Luengo-Gutierrez, L., Chadwick, J.S., Kong, G., Zhou, L., Crawford, G., Danzi, M.C., Myridakis, A., Brandis, A., Bello, A.T., et al. (2022). The gut metabolite indole-3 propionate promotes nerve regeneration and repair. Nature *607*, 585–592.
28. Zhang, Z., Mu, X., Cao, Q., Shi, Y., Hu, X., and Zheng, H. (2022). Honeybee gut *Lactobacillus* modulates host learning and memory behaviors via regulating tryptophan metabolism. Nat. Commun. *13*, 2037.
29. Goldstein, J., and Steiner, U.K. (2020). Ecological drivers of jellyfish blooms - The complex life history of a "well-known" medusa (*Aurelia aurita*). J. Anim. Ecol. *89*, 910–920.
30. Kroiher, M., Siefker, B., and Berking, S. (2000). Induction of segmentation in polyps of *Aurelia aurita* (Scyphozoa, Cnidaria) into medusae and formation of mirror-image medusa anlagen. Int. J. Dev. Biol. *44*, 485–490.
31. Wiebring, A., Helmholz, H., Sötje, I., Lassen, S., Prange, A., and Tiemann, H. (2010). A New Method for the Separation of Different Types of Nematocysts from Scyphozoa and Investigation of Proteinaceous Toxins Utilizing Laser Catapulting and Subsequent Mass Spectrometry. Mar. Biotechnol. *12*, 308–317.
32. Sunagar, K., Columbus-Shenkar, Y.Y., Fridrich, A., Gutkovich, N., Aharoni, R., and Moran, Y. (2018). Cell type-specific expression profiling unravels the development and evolution of stinging cells in sea anemone. BMC Biol. *16*, 108.
33. Babonis, L.S., and Martindale, M.Q. (2017). PaxA, but not PaxC, is required for cnidocyte development in the sea anemone *Nematostella vectensis*. EvoDevo *8*, 14.
34. Rachamim, T., Morgenstern, D., Aharonovich, D., Brekhman, V., Lotan, T., and Sher, D. (2015). The dynamically evolving nematocyst content of an anthozoan, a scyphozoan, and a hydrozoan. Mol. Biol. Evol. *32*, 740–753.
35. Gold, D.A., Lau, C.L.F., Fuong, H., Kao, G., Hartenstein, V., and Jacobs, D.K. (2019). Mechanisms of cnidocyte development in the moon jellyfish *Aurelia*. Evol. Dev. *21*, 72–81.
36. Li, R., Yu, H., Xue, W., Yue, Y., Liu, S., Xing, R., and Li, P. (2014). Jellyfish venomics and venom gland transcriptomics analysis of *Stomolophus meleagris* to reveal the toxins associated with sting. J. Proteomics *106*, 17–29.
37. Gold, D.A., Katsuki, T., Li, Y., Yan, X., Regulski, M., Ibberson, D., Holstein, T., Steele, R.E., Jacobs, D.K., and Greenspan, R.J. (2019). The genome of the jellyfish *Aurelia* and the evolution of animal complexity. Nat. Ecol. Evol. *3*, 96–104.
38. Murillo-Rincon, A.P., Klimovich, A., Pemöller, E., Taubenheim, J., Mortzfeld, B., Augustin, R., and Bosch, T.C.G. (2017). Spontaneous body contractions are modulated by the microbiome of *Hydra*. Sci. Rep. *7*, 15937.
39. Mohamed, N.M., Colman, A.S., Tal, Y., and Hill, R.T. (2008). Diversity and expression of nitrogen fixation genes in bacterial symbionts of marine sponges. Environ. Microbiol. *10*, 2910–2921.
40. Usher, K.M. (2008). The ecology and phylogeny of cyanobacterial symbionts in sponges. Mar. Ecol. *29*, 178–192.
41. Gao, Z.M., Zhou, G.W., Huang, H., and Wang, Y. (2017). The Cyanobacteria-Dominated Sponge *Dactylospongia elegans* in the South China Sea: Prokaryotic Community and Metagenomic Insights. Front. Microbiol. *8*, 1387.
42. Lesser, M.P., Mazel, C.H., Gorbunov, M.Y., and Falkowski, P.G. (2004). Discovery of symbiotic nitrogen-fixing cyanobacteria in corals. Science *305*, 997–1000.
43. Kojima, A., and Hirose, E. (2012). Transmission of Cyanobacterial Symbionts During Embryogenesis in the Coral Reef Ascidians *Trididemnum nubilum* and *T. clinides* (Didemnidae, Ascidiacea, Chordata). Biol. Bull. *222*, 63–73.
44. Lopez-Guzman, M., Erwin, P.M., Hirose, E., and López-Legentil, S. (2020). Biogeography and host-specificity of cyanobacterial symbionts in colonial ascidians of the genus *Lissoclinum*. Syst. Biodivers. *18*, 496–509.
45. Daley, M.C., Urban-Rich, J., and Moisander, P.H. (2016). Bacterial associations with the hydromedusa *Nemopsis bachei* and scyphomedusa *Aurelia aurita* from the North Atlantic Ocean. Mar. Biol. Res. *12*, 1088–1100.
46. Kos Kramar, M., Tinta, T., Lučić, D., Malej, A., and Turk, V. (2019). Bacteria associated with moon jellyfish during bloom and post-bloom periods in the Gulf of Trieste (northern Adriatic). PLoS One *14*, e0198056.
47. Basso, L., Rizzo, L., Marzano, M., Intranuovo, M., Fosso, B., Pesole, G., Piraino, S., and Stabili, L. (2019). Jellyfish summer outbreaks as bacterial vectors and potential hazards for marine animals and humans health? The case of *Rhizostoma pulmo* (Scyphozoa, Cnidaria). Sci. Total Environ. *692*, 305–318.
48. Stabili, L., Rizzo, L., Basso, L., Marzano, M., Fosso, B., Pesole, G., and Piraino, S. (2020). The Microbial Community Associated with *Rhizostoma pulmo*: Ecological Significance and Potential Consequences for Marine Organisms and Human Health. Mar. Drugs *18*, 437.
49. Wu, X., Jiang, J., Wan, Y., Giesy, J.P., and Hu, J. (2012). Cyanobacteria blooms produce teratogenic retinoic acids. Proc. Natl. Acad. Sci. *109*, 9477–9482.
50. Millard, A., Scanlan, D.J., Gallagher, C., Marsh, A., and Taylor, P.C. (2014). Unexpected evolutionary proximity of eukaryotic and cyanobacterial enzymes responsible for biosynthesis of retinoic acid and its oxidation. Mol. Biosyst. *10*, 380–383.
51. Jaja-Chimedza, A., Sanchez, K., Gantar, M., Gibbs, P., Schmale, M., and Berry, J.P. (2017). Carotenoid glycosides from cyanobacteria are teratogenic in the zebrafish (*Danio rerio*) embryo model. Chemosphere *174*, 478–489.
52. Sehnal, L., Smutná, M., Bláhová, L., Babica, P., Šplíchalová, P., and Hilscherová, K. (2022). The Origin of Teratogenic Retinoids in Cyanobacteria. Toxins *14*, 636.
53. Ruch, S., Beyer, P., Ernst, H., and Al-Babili, S. (2005). Retinal biosynthesis in Eubacteria: in vitro characterization of a novel carotenoid oxygenase from *Synechocystis* sp PCC 6803. Mol. Microbiol. *55*, 1015–1024.
54. Sugiyama, K., and Takaichi, S. (2020). Carotenogenesis in cyanobacteria: CruA/CruP-type and CrtL-type lycopene cyclases. J. Gen. Appl. Microbiol. *66*, 53–58.
55. Lesser, M.P., and Stochaj, W.R. (1990). Photoadaptation and Protection against Active Forms of Oxygen in the Symbiotic Procaryote *Prochloron* sp. and Its Ascidian Host. Appl. Environ. Microbiol. *56*, 1530–1535.
56. David, C.N., Ozbek, S., Adamczyk, P., Meier, S., Pauly, B., Chapman, J., Hwang, J.S., Gojobori, T., and Holstein, T.W. (2008). Evolution of complex structures: minicollagens shape the cnidarian nematocyst. Trends Genet. *24*, 431–438.
57. Babonis, L.S., Enjolras, C., Ryan, J.F., and Martindale, M.Q. (2022). A novel regulatory gene promotes novel cell fate by suppressing ancestral fate in the sea anemone *Nematostella vectensis*. Proc. Natl. Acad. Sci. USA *119*, e2113701119.
58. Rolig, A.S., Mittge, E.K., Ganz, J., Troll, J.V., Melancon, E., Wiles, T.J., Alligood, K., Stephens, W.Z., Eisen, J.S., and Guillemin, K. (2017). The enteric nervous system promotes intestinal health by constraining microbiota composition. PLoS Biol. *15*, e2000689.
59. Jia, Y., Jin, S., Hu, K., Geng, L., Han, C., Kang, R., Pang, Y., Ling, E., Tan, E.K., Pan, Y., and Liu, W. (2021). Gut microbiome modulates *Drosophila* aggression through octopamine signaling. Nat. Commun. *12*, 2698.
60. Hay, S. (2006). Marine ecology: Gelatinous bells may ring change in marine ecosystems. Curr. Biol. *16*, R679–R682.
61. Ruzicka, J.J., Brodeur, R.D., and Wainwright, T.C. (2007). Seasonal food web models for the oregon inner-shelf ecosystem: Investigating the role of large jellyfish. Calif. Coop. Ocean. Fish. Investig. Rep. *48*, 106–128.
62. Helm, R.R. (2018). Evolution and development of scyphozoan jellyfish. Biol. Rev. *93*, 1228–1250.
63. Murillo-Rincón, A.P. (2017). Modulation of neuronal activity by symbiotic bacteria in the early-branching metazoan *Hydra*. ProQuest. https://www.proquest.com/docview/2014991111?pq-origsite=wos&accountid=178610.
64. Sun, T., Luo, Z., Peng, S., Schiariti, A., Du, C., Zhao, J., and Dong, Z. (2023). Physiological response of *Aurelia coerulea* polyps to elevated seasonal temperatures. Hydrobiologia *850*, 2005–2014.
65. Douglas, G.M., Maffei, V.J., Zaneveld, J.R., Yurgel, S.N., Brown, J.R., Taylor, C.M., Huttenhower, C., and Langille, M.G.I. (2020). PICRUSt2 for prediction of metagenome functions. Nat. Biotechnol. *38*, 685–688.
66. Kim, D., Langmead, B., and Salzberg, S.L. (2015). HISAT: a fast spliced aligner with low memory requirements. Nat. Methods *12*, 357–360.
67. Pertea, M., Pertea, G.M., Antonescu, C.M., Chang, T.C., Mendell, J.T., and Salzberg, S.L. (2015). StringTie enables improved reconstruction of a transcriptome from RNA-seq reads. Nat. Biotechnol. *33*, 290–295.
68. Wang, J., Zhang, T., Shen, X., Liu, J., Zhao, D., Sun, Y., Wang, L., Liu, Y., Gong, X., Liu, Y., et al. (2016). Serum metabolomics for early diagnosis of esophageal squamous cell carcinoma by UHPLC-QTOF/MS. Metabolomics *12*, 116.

STAR★METHODS

KEY RESOURCES TABLE

REAGENT or RESOURCE	SOURCE	IDENTIFIER
Chemicals, peptides, and recombinant proteins		
Ampicillin	Macklin	A800429-5g
Chloramphenicol	Macklin	C804169-5g
Neomycin	BBI	A610366-0025
Streptomycin	ACMEC	S28790-5g
Rifampin	Macklin	R6056-5g
Spectinomycin	Macklin	S6106-5g
Amphotericin B	Yuanye	S26954-100mg
Sodium Hypochlorite	Macklin	S817439-2.5L
Dispase 2	Coolaber	CD4691-1g
Collagenase 3	ACMEC	C12702
Fetal Bovine Serum	Gibco	TZTJ10099
4% Paraformaldehyde	Biosharp	BL539A500
Calcein AM	BD	564061
Draq7™	BD	564904
Critical commercial assays		
DNeasy PowerSoil Pro Kit	QIAGEN	47016
Polysaccharide and Polyphenol RNA extraction kit	ZOMANBIO	ZP411C-2
Hieff NGS Ultima Dual-mode mRNA Library Prep Kit	YEASEN	12309ES08
TruSeq DNA Sample Prep Kit	Illumina	FC-121-2002
Qubit High-Sensitivity DNA Assay Kit	Invitrogen	Q32851
Deposited data		
Raw transcriptomics data	NCBI	BioProject: PRJNA1013748
Raw 16S rRNA gene sequencing data	NCBI	BioProject: PRJNA1013424
Raw single-cell RNA sequencing data	NCBI	BioProject: PRJNA1014937
Oligonucleotides		
Primer 27F 5′-AGAGTTTGATCMTGGCTCAG-3′	Sangon Biotech	N/A
Primer 1492R 5′-GGTTACCTTGTTACGACTT-3′	Sangon Biotech	N/A
515F 5′-GTGCCAGCMGCCGCGG-3′	Sangon Biotech	N/A
806R 5′-GGACTACHVGGGTWTCTAAT-3′	Sangon Biotech	N/A
Software and algorithms		
Optec OPTPro 2008 software	Optec	N/A
Flash version 1.2.11	Flash	N/A
Uparse version 7.0.1090	Uparse	N/A
RDP classifier version 2.11	RDP classifier	N/A
Mothur version 1.30.2	Mothur	N/A
R version 3.3.1	R	N/A
PICRUSt2	N/A	N/A
HISAT2 tools version 2.2.1	HISAT2	N/A
StringTie version 2.2.1	StringTie	N/A
DESeq2 version 1.30.1	DESeq2	N/A

(*Continued on next page*)

Continued

REAGENT or RESOURCE	SOURCE	IDENTIFIER
R/clusterProfiler version 4.4.4	clusterProfiler	N/A
Progenesis QI	N/A	N/A
BD Rhapsody™ WTA Analysis Pipeline version 4.1	BD Rhapsody™	N/A
R version 3.6.2	R	N/A
R/Seurat version 4.0.6	Seurat	N/A
R/Doublefinder	Doublefinder	N/A
R/SCTransform	SCTransform	N/A
IBM SPSS statistics 25	IBM	N/A
OriginPro 2021	Origin	N/A

RESOURCE AVAILABILITY

Lead contact

Further information and requests for resources and reagents should be directed to and will be fulfilled by the lead contact, Zhijun Dong (zjdong@yic.ac.cn).

Materials availability

This study did not generate unique reagents.

Data and code availability

- Raw transcriptomics data, 16S rRNA gene sequencing data, and single-cell RNA sequencing data have been deposited at the NCBI database and are publicly available as of the date of publication. Accession numbers are listed in the key resources table.
- All original code is available in this paper's supplemental information, and we performed other bioinformatics analysis on the BMKCloud platform (www.biocloud.net), Majorbio Cloud Platform (www.majorbio.com) and OmicShare tools (https://www.omicshare.com/tools).
- Any additional information required to reanalyze the data reported in this paper is available from the lead contact upon request.

EXPERIMENTAL MODEL AND STUDY PARTICIPANT DETAILS

Animal use ethics

All animal experiments were conducted per the guidelines and approval of the Yantai Institute of Coastal Zone Research, Chinese Academy of Sciences (KJ-LL-003).

Husbandry of *Aurelia coerulea*

The native polyps of *A. coerulea* were maintained in 1.5-liter covered acrylic tanks under dark conditions in a 19°C incubator for a month. The polyps were fed three times a week with freshly hatched *Artemia* nauplii and replaced seawater with fresh natural seawater 2–4 h after feeding.

Generation of sterile *Artemia* nauplii

The treatment methods for sterile *Artemia* are described by Murillo Rincon,[63] with minor modifications. Specifically, *Artemia salina* cysts (~1 g) were hydrated in a beaker containing 90 ml sterile Milli-Q water at room temperature for 1h. Subsequently, 50 ml sodium hypochlorite and 3.3 ml 32% NaOH solution were added, gently shaken and incubated for 6 min until the *Artemia* cysts became orange. 70 ml $Na_2S_2O_3$ solution (10 mg/L) was used to terminate the reaction. Immediately, the naked cysts were rinsed with 3 L sterile Mill-Q water on a 100 μm sterile sieve to completely remove the bleaching solution. Finally, the treated cysts were recoiled into a 1 L sterile conical flask with 500 mL of sterile ASW (artificial seawater, prepared from reef crystals to salinity 30 ppt and then filtered through 0.22 μm filter membranes), covered with sterile sealing film and incubated in an oscillating incubator under light conditions, 27°C and 160 rpm for 24 h. To check the sterile state of the hatched nauplii, 60 μl hatchlings after homogenization were plated into 2216E plate. Lack of bacterial growth after 3 d of incubation in 19°C was observed. The genomic DNA of nauplii extracted with a DNeasy PowerSoil Pro Kit (QIAGEN, Germany) was used as the template for 16S rRNA gene PCR amplification with primers 27F (5′-AGAGTTTGATCMTGGCTCAG-3′) and 1492R (5′-GGTTACCTTGTTACGACTT-3′). The absence of bands was considered as proof of a sterile state.

Generation of control, antibiotic-treated and recolonized polyps

Healthy polyps (n = 9000) were selected and re-settled in nine acrylic tanks with a volume of 1.5 L, each containing 1 L of sterile ASW. Another batch (n = 720) was prepared in 15 48-well sterile cell plates with a single well containing 1 mL of sterile ASW. Control polyps were generated from healthy polyps after re-settlement in three tanks (n = 3000 polyps) and five 48-well plates (n = 240 polyps). Antibiotic-treated polyps were established by treating healthy polyps with an antibiotic mixture in six 1.5 L tanks (n = 6000 polyps) and ten 48-well plates (n = 480 polyps). The antibiotic mixture was added to one members based on Jensen et al.[25] and contained 50 mg/L ampicillin (Macklin, China), chloramphenicol (Macklin, China), neomycin (BBI, China), streptomycin (ACMEC, China), rifampin (Macklin, China), 60 mg/L spectinomycin (Macklin, China), and 25 mg/L amphotericin B (Yuanye, China) solubilized in sterile ASW. The antibiotic treatment was performed at 19°C for 7 d, during which new antibiotic mixture were replaced daily. The reduction in the microbiota was tested by 16S rRNA gene PCR amplification with primers 27F and 1492R and was characterized by the shallowing of the band. The templates were the genomic DNA of the control and antibiotic-treated polyps extracted using the DNeasy PowerSoil Pro Kit (QIAGEN, Germany). Another proof of the decrease in microbiota was that the CFU on 2216E plates plated with two homogenized antibiotic-treated polyps was reduced by 90% ~ 97% than control polyps after 3 d of incubation in 19°C.

Recolonized polyps were conducted with one-half of the aforementioned antibiotic-treated polyps. The method was performed as described by Weiland-Bräuer et al.,[12] with minor modifications. Briefly, ten control polyps starved for 3 d were washed three times with 1 ml sterile ASW in a 1.5-ml centrifuge tube. Sterile ASW (1 ml) was added to the tube, and homogenization was performed using a T10 basic ULTRA-TURRAX homogenizer (IKA, Germany) for 20 s. The homogenate was filtered with a 5 μm syringe filter to remove eukaryotic cells. Then, the filtered homogenate was diluted gradients, and 40 μl of each diluent was coated on a 2216E plate. After incubation at 19°C for 48 h, CFU was counted, and the bacterial CFU in each 1 ml homogenate was estimated. Subsequently, 10 ml of the filtered homogenate (2.55×10^5 cells/mL) following the above procedure were added into each of three 1.5 L tanks (n = 3000 polyps) and 10 μl into each well of five 48-well plates (n = 240 polyps) for recolonization. The polyps were exposed in 19°C for 48 h and new sterile ASW with the homogenate was replaced daily. Finally, the incubated animals, as recolonized polyps, were returned to the sterile ASW. Recolonized polyps were sampled for 16S rRNA gene sequencing to examine recolonization effects.

METHOD DETAILS

Physiological parameters

The control, antibiotic-treated and recolonized polyps of *A. coerulea* were cooled from 19°C to 12°C to induce strobilation, and a 48-day physiological monitoring was carried out from the date of decreasing temperature (Day 0). During the experiment, all polyps were fed a sufficient amount of newly hatched sterile *Artemia* nauplii once a week, and sterile ASW was replaced 4 h after feeding. The process of strobilation of polyps in the 48-well plates was observed every 3 d under each treatment condition. The onset of strobilation initiation, progression to the advanced stage, and the maximum count of segments and ephyrae released were individually documented for each polyp. The total number of strobilae in each 48-well plate as one replicate (n = 5 replicates/treatment) was counted every 3 d to calculate the relative abundance of strobilae (%), defined as the ratio of the number of strobilae to that of surviving individuals per plate. The relative abundance of strobilae that released ephyrae (%) was obtained as the ratio of the number of advanced strobilae to that of surviving individuals per plate (n = 5 replicates/treatment). The mean number of segments and ephyrae released per strobila was calculated as the average of the maximum number of segments and ephyrae of surviving individuals in each 48-well plate (n = 5 replicates/treatment).

The length and width (excluding tentacles) of 30 polyps each treatment were measured on day 3 at 12°C, and the size of each polyp was determined by the multiplication of length and width, which was defined by Weiland-Bräuer et al.[12] On day three, the feeding rate of the polyps was also determined. Briefly, a single polyp settled in a single well of a 48-well plate was fed 20 newly hatched sterile *Artemia* nauplii. After feeding for 1 h, the remaining number was counted. The carbon content estimation method of each nauplii was based on the description of Sun et al.[64] and was quantified as 1.95×10^{-3} mg/ind. The feeding rate (mgC ind^{-1} h^{-1}) was designated as the carbon intake per hour per polyp, and 30 polyps were measured on each treatment. On the day 36 at 12°C, the size and feeding rate of newly released ephyrae in three treatments were quantified, and 30 animals in each treatment were measured. The methods employed to determine the two parameters for ephyrae were fundamentally identical to those employed for polyps. However, a modification was made to the measurement of the feeding rate by substituting the 48-well plate with 6-well plates, each well filled with 10 ml of sterile ASW. The feeding rate of the ephyrae was measured continuously for 3 d, once a day, and the size of the ephyrae was measured simultaneously on day 3. During the 48-day experiment, the morphology of animals at different stages in each treatment was captured using a ZEISS STEMI 508 microscope (Germany) with an Optec CCD TP510 camera (USA), and images captured using the Optec OPTPro 2008 software were obtained as the output.

Sample collection of multi-omics sequencing

To fully explore the microbial community associated with *Aurelia* throughout the strobilation experiment, samples from four stages (polyp, early strobila, advanced strobila and ephyra) in the control and antibiotic-treated groups were collected for 16S rRNA gene amplicon sequencing, and recolonized polyps were also collected for 16S rRNA gene amplicon sequencing. Furthermore, samples of the control and antibiotic-treated organisms were successively collected at four stages for transcriptome sequencing and metabolomic sequencing to comprehensively analyze the relationship between microbial changes and host physiological phenotypes at two levels. The collected staged omics samples were as follows: control polyps (CP), antibiotic-treated polyps (AP) and recolonized polyps (RP) sampled in day 3;

control early strobilae (CES) sampled in day 21, and antibiotic-treated early strobilae (AES) in day 35; control advanced strobilae (CAS) sampled in day 28, and antibiotic-treated advanced strobilae (AAS) in day 39; as well as control ephyrae (CE) sampled in day 28, and antibiotic-treated ephyrae (AE) in day 39.

In the 48-day experiment, the strobilation process of the antibiotic treatment was delayed compared to that of the control and recolonized treatments. To reveal the reasons for the delay, we additionally collected samples of the antibiotic-treated animals (ACES and ACAS) at the same time when the control and recolonized groups reached the early strobilae (day 21) and the advanced strobilae (day 28) and performed multi-omics sequencing (16S rRNA gene sequencing, RNA sequencing and LC-MS analysis).

16S rRNA gene amplicon sequencing and data analysis

Genomic DNA was extracted using a DNeasy PowerSoil Pro Kit (QIAGEN, Germany) according to the manufacturer's instructions, with minor modifications. Each DNA sample was extracted from five animals, with three replicates per group. The extracted DNA samples were tested using 1% agarose gel electrophoresis. DNA templates (10 ng) were subjected to PCR with a 20-μl total volume by using a TransGen AP221-02 (Trans, China). Cycling conditions were initial denaturation at 95°C for 3 min, followed by 29 cycles of 30 s at 95°C, 30 s at 53°C, and 45 s at 72°C, and finally 10 min at 72°C, and they were performed on ABI GeneAmp® 9700 System (USA). The following universal PCR primers (515F, 5′-GTGCCAGCMGCCGCGG-3′; 806R, 5′-GGACTACHVGGGTWTCTAAT-3′) with barcode directed at the V4 region of bacterial and archaeal rRNA genes were used to generate libraries. All PCRs were carried out in triplicate and mixed PCR products were detected by 2% agarose gel electrophoresis. Subsequently, the PCR products were quantified using the QuantiFluorTM-ST Blue Fluorescence Quantification System (Promega) and normalized to equimolar amounts. The amplicon libraries were generated using a TruSeq DNA Sample Prep Kit and sequenced using the Illumina MiSeq (PE300) platform at Majorbio Bio-Pharm Technology Co., Ltd (Shanghai, China).

Paired-end reads were spliced using Flash (version 1.2.11). Operational taxonomic units (OTUs) were clustered with a 97% sequence similarity cutoff using Uparse (version 7.0.1090; http://drive5.com/uparse/). The Bayesian algorithm of the RDP classifier (version 2.11) was used to compare OTU sequences based on Silva (Release138, http://www.arb-silva.de), and the classification confidence was set to 0.7. All samples were rarefied to the sequence number corresponding to the sample with the least number of sequences. Moreover, α diversity analyses were carried out using mothur (version 1.30.2, https://mothur.org/wiki/calculators/). The β diversity was characterized by principal co-ordinates analysis (PCoA analysis) based on unweighted unifrac distance, visualized by R (version 3.3.1), and analyzed for community structure differences based on adonis tests (permutation number = 999). LEfSe analysis was used to screen for biomarkers between the groups according to a threshold LDA score >4. Finally, PICRUSt2 (https://github.com/picrust/picrust2) was used to predict potential functions of the microbiota.[65]

Transcriptome sequencing and analysis

RNA was isolated using a polysaccharide and polyphenol RNA extraction kit (ZOMANBIO, China) according to the manufacturer's instructions, with minor modifications. Preliminary experiments showed that the kit was superior to several traditional methods in terms of the efficiency of total RNA extraction from jellyfish with high polysaccharide content. Briefly, each RNA sample was extracted from 20 animals, with three replicates per group. The samples were frozen in liquid nitrogen and stored at −80°C, and then operated according to the kit instructions. A NanoDrop 2000 spectrophotometer (Thermo Fisher Scientific, USA) was used to detect the purity and concentration of RNA, and an Agilent 2100 Bioanalyzer/Caliper LabChip GX (Agilent Technologies, USA) was used to accurately detect the integrity of RNA. A cDNA library was prepared using a Hieff NGS Ultima Dual-mode mRNA Library Prep Kit (Illumina). Quality control of the library was performed using a Qubit 3.0 fluorescence quantitative instrument (Thermo Fisher Scientific, USA) to preliminarily quantify the results of the Qsep400 high-throughput analysis system (BiOptic Inc., China) that was performed to detect the insertion fragment of the library. Q-PCR method was used to accurately quantify the effective concentration of the library. The qualified library was sequenced in the PE150 mode using the Illumina NovaSeq6000 sequencing platform at Biomarker Technologies Co., Ltd. (Beijing, China).

Adapters and bad-quality reads were removed from the raw reads to obtain clean reads. The clean reads were quickly and accurately mapped to our own reference genome (NCBI BioProject: PRJNA1005405) using HISAT2 tools (version 2.2.1),[66] and then assembled using StringTie (version 2.2.1).[67] Gene expression levels were estimated as fragments per kilobase of transcript per million mapped fragments (FPKM). The differentially expressed gene (DEG) analysis was performed using DESeq2 software (version 1.30.1), with Fold Change ≥ 1.5 and *P*-adjusted (FDR) < 0.01 as the screening criteria. Furthermore, GO and KEGG pathway enrichment analyses of DEGs were implemented using clusterProfiler packages (version 4.4.4) based on the Wallenius non-central hyper-geometric distribution.

LC-MS analysis

Each metabolomic sample was extracted from 80 animals with eight replicates per group. The LC-MS system comprised Waters Acquity I-Class PLUS ultra-high-performance liquid tandem Waters Xevo G2-XS QTOF high-resolution mass spectrometer. Primary and secondary mass spectrometry data were collected in MSe mode under the control of acquisition software (MassLynx V4.2, Waters) using a Waters Xevo G2-XS QTOF high-resolution mass spectrometer. LC-MS analysis was performed as described by Wang et al.[68] with a few modifications. Briefly, the separation elution was 0.1% formic acid aqueous solution (A) and 0.1% formic acid acetonitrile (B) at a flow rate of 400 μL/min. Samples were automatically injected at a volume of 1 μl. The main parameters were listed as follows: capillary voltage, 2000 V (positive ion mode) or 1500 V (negative ion mode); cone voltage, 30 V; ion source temperature, 150°C; desolvent gas temperature, 500°C; backflush gas flow rate, 50 L/h; desolventizing gas flow rate, 800 L/h.

The acquired raw data were processed using the Progenesis QI software for baseline filtering, peak extraction, peak alignment, and normalization. The differential metabolites were screened using the OPLS-DA model based on the following criteria: fold change >1, p value <0.05, and VIP value > 1. The p value was calculated using the Student's *t* test. The KEGG pathway enrichment significance of the different metabolites was calculated using clusterProfiler packages (version 4.4.4) based on the Wallenius non-central hypergeometric distribution.

Single-cell RNA sequencing

To prepare the scRNA-seq library, eight control ephyrae were collected and washed twice in Ca^{2+}-and Mg^{2+}-free ASW (CMFASW). Samples were immediately transferred to 2 ml of digestive buffer (3.6 mg/ml Dispase 2 and 1.25 mg/ml collagenase 3 in CMFASW). Dissociation was carried out at room temperature for 20 min with occasional disruption and subsequently stopped by adding 8% volume of fetal bovine serum. After dissociation, the single-cell suspension was centrifuged at 500 × g for 5 min at 4°C, resuspended in pre-chilled CMFASW, and subsequently filtered through a 40-μm cell strainer (FALCON). Low concentrations of Calcein AM (2 mM) and Draq7™ (0.3 mM) were used to measure cell viability. Only cell suspensions with >90% viability were used for cell capture. A BD Rhapsody system was used to capture single cells and construct libraries. Libraries were quantified using a Qubit High-Sensitivity DNA Assay Kit (Invitrogen). Sequencing was performed using a NovaSeq sequencer (Annon Technologies) with 150-bp paired-end runs.

Fastq files were processed using the BD Rhapsody™ WTA Analysis Pipeline (version 4.1) on Seven Bridges (https://www.sevenbridges.com) following the manufacturer's guidelines. The reads were mapped to the *Aurelia* genome (NCBI BioProject: PRJNA1005405). Unique molecular identifier (UMI) count matrices were imported into R (version 3.6.2) and processed using the R package Seurat (version 4.0.6) (https://satijalab.org/seurat/). To remove ambient RNA contamination and putative doublets, low-quality transcriptomes were filtered for the sample as follows:1) cells with less than 400 or more than 2000 expressed genes were discarded, 2) only genes that were expressed in at least three cells in each dataset were considered, and 3) cells were filtered out based on total UMI counts, excluding cells with low (<500) or large numbers (>10000) of UMIs. The Doublefinder package was used to remove putative doublets. For generating cell type clusters, the SCTransform package with default parameter was used for data standardization. Following the standard downstream processing steps, we ran a principal component analysis and UMAP in 30 dimensions. FindNeighbors (dimensions 1:30) and FindClusters (resolution 0.1) were run to generate the cell clusters. The FindAllMarker of the Seurat (version 4.0.6) was used to generate the gene expression matrix for each cluster.

Nematocyte imaging and quantification

The samples used for the morphological imaging of nematocytes were polyps and ephyrae on day three after release. Animals were fixed in pre-cooled 4% paraformaldehyde for 1 h, transferred to a glass slide, and photographed under an Olympus BX51 microscope (Japan). The number of nematocytes was counted using a Leica DMi8 microscope (Germany), and 20 animals were counted in each treatment group. The sample collection and fixation methods were the same as those used for morphological imaging. The counting range of the number of nematocytes in each polyp was a rectangular area (150 × 50 μm) at an extended tentacle base, while that in each ephyra was a rectangular area (300 × 350 μm) at a flat marginal lappet base.

QUANTIFICATION AND STATISTICAL ANALYSIS

Results were graphed as mean ± SD, except for the feeding rate of ephyrae, which was calculated as mean ± SE. Statistical analyses were performed using IBM SPSS Statistics 25 and OriginPro 2021. One-way ANOVA and Fisher's LSD test were used to evaluate the differences in physiological parameters and the number of nematocytes among the control, antibiotic-treated and recolonized treatments. The differences in the Chao1 index were tested using the Student's *t* test.